Article

Two Prism Critical Angle Refractometry with Attenuating Media

Spyridon Koutsoumpos, Panagiotis Giannios [ID] and Konstantinos Moutzouris *[ID]

Laboratory of Electronic Devices and Materials, Department of Electrical & Electronic Engineering, University of West Attica, 12244 Egaleo, Greece; skoutsoumpos@uniwa.gr (S.K.); panagiotis.giannios@irbbarcelona.org (P.G.)
* Correspondence: moutzouris@uniwa.gr

Abstract: We present a concept that enables the determination of the complex refractive index of attenuating media from two critical angles, measured sequentially at two interfaces between a single sample and two different prisms. The proposed method is general in that it applies with *s* and *p* polarisation states, thus it is suited for the characterisation of isotropic as well as anisotropic media. Uncertainty analysis indicates that relative error in the determination of the real (imaginary) index can be less than 10^{-4} (in the order of 10%), respectively.

Keywords: complex refractive index; total internal reflection; optical instruments

1. Introduction

The refractive index of a medium derives from the reflectance profile at an interface between the sample and a front reference medium, which is typically a transparent prism [1,2]. When the sample is transparent, the refractive index is a real number that can be determined from just one out of several features of the reflectance profile, such as the critical angle of total internal reflection (θ_c) [3–5] or the Brewster angle (θ_B) [6–9]. When the sample attenuates light, the refractive index becomes a complex quantity, the imaginary part of which incorporates light extinction properties (absorption and/or scattering). Then, a pair of input values is needed to recover the real and imaginary component. This pair may comprise, for example, the critical angle of attenuated total reflection along with the reflectance at that point (θ_c, R_c) [10,11], the *pseudo*-Brewster angle together with the reflectance at that point (θ_B, R_B) [12], or the the pseudo-Brewster angle and the reflectance at normal incidence ($\theta_B, R_\perp$) [13].

Typical prism-coupling refractometers [14–17] are equipped with high resolution rotary tables (see Figure 1a). Hence, the angular features of the reflectance profile (e.g., θ_c) can be resolved with high accuracy [18]. On the contrary, accuracy in the measurement of reflectance (e.g., R_c) is seriously compromised by unavoidable laser power fluctuations [18,19]. In that respect, it is advantageous to devise methods whereby the complex refractive index results from an input pair that contains two angles.

Here, we demonstrate how to retrieve the complex optical constant $n_r + i \cdot n_i$ of an attenuating medium from the critical angle pair (θ_c, θ_c') measured at two interfaces between the same sample and two different prisms. The real indices of the prisms are n_p and n_p', such that $n_p/n_p' = \Lambda$. To obtain a first insight, Figure 1b depicts corresponding reflectance profiles. Calculations are based on the Fresnel equation for the exemplary case of *s* polarised light, while parameters

$$n = \frac{n_r}{n_p}, \quad k = \frac{n_i}{n_p}, \quad n' = \frac{n_r}{n_p'} = n\Lambda, \quad k' = \frac{n_i}{n_p'} = k\Lambda \tag{1}$$

assume the values that are indicated in the figure's caption. Located at the maximum of the respective reflectance derivative $dR/d\theta$, which is also plotted in Figure 1b, critical angles θ_c and θ_c' are separated by $\Delta = \theta_c - \theta_c'$. Reflectances R_c and R_c' are also tracked in Figure 1b.

Figure 1. (**a**) A typical prism-coupling refractometer. The sample is attached to the base of a transparent reference prism, which sits on a rotary table. Incoming through the prism's front facet, a collimated linearly polarized laser beam hits the interface at a variable incidence angle θ. The reflected light exits the prism through its rear facet, heading towards a photodiode (PD), where the reflectance profile $R(\theta)$ is monitored. (**b**) Fresnel reflectance profiles $R(\theta)$ at two interfaces between a sample and two different prisms. Bell-like curves are corresponding derivatives $dR/d\theta$, peaking at θ_c and θ'_c. Calculations assume s polarisation and $n = 0.75$, $k = 5 \cdot 10^{-3}$, $\Lambda = 1.2$.

The sample's complex refractive index derives from the input pair (θ_c, θ'_c) as the unique numerical solution of a well-posed equation system that is fully described next. The proposed method is general in the sense that it applies with s and p polarised light, hence it is suited for isotropic as well as anisotropic media. Uncertainty analysis indicates that within an extinction range, say, $0.001 < k < 0.01$, which includes several material families of interest, the real (or the imaginary) index can be determined with relative error less than $\sim 10^{-4}$ (or $\sim 10\%$), respectively.

The proposed method resembles the two prism, two angle approach introduced by Azzam several decades ago [20], utilizing the pseudo-Brewster angle pair (θ_B, θ'_B) as input. Despite the conceptual similarity, Azzam's routine was found to be inaccurate (or even unusable) when $n_i/n_r \ll 1$, a condition that automatically excludes most non-metal samples (The review of literature within the space limits of this letter is not exhaustive. For example, the interested reader should be referred to Hirschfeld's two prism method, which is based on the measurement of two reflectances (R, R') at preset angles [21]. Another report on single prism two angle method [22] was also published recently, lacking however generality, since it applies only to isotropic media. Finally, we acknowledge a conceptually different route to determine the complex optical constants of attenuating samples, which depends on fitting experimental data $R(\theta)$ to Fresnel equations [23–28]. This approach is not a "point" method and has been proven sensitive to the choice of fit range [29,30]. An indepth comparison of the proposed method to Fresnel fitting is beyond our current scopes).

2. Background Theory

We start by recalling the mathematical framework that is derived from Fresnel equations in Ref. [10]. The involved formulas are compactly expressed in terms of the real dielectric constant of the prism $\epsilon_p = n_p^2$ and the complex dielectric constant of the sample $\epsilon_r + i \cdot \epsilon_i = (n_r + i \cdot n_i)^2$. Shorthands t and ρ, which relate to θ_c and R_c via

$$t = \tan \theta_c \quad \text{and} \quad \rho = \frac{1 + R_c}{1 - R_c} \tag{2}$$

are also convenient. Then, it is

$$\frac{\epsilon_r}{\epsilon_p} = \frac{\alpha + t^2}{1 + t^2} \quad \text{and} \quad \frac{\epsilon_i}{\epsilon_p} = \frac{\sqrt{\gamma^2 - \alpha^2}}{1 + t^2}. \tag{3}$$

Parameters α and γ depend on polarisation. Analytic solutions exist for s polarisation. These are

$$\gamma = \frac{2t}{(3\rho^2 - 2\rho - 2)t + \rho\sqrt{(9\rho^2 - 12\rho - 8)t^2 - 4}}, \tag{4}$$

$$\alpha = \frac{(1 + \gamma)^2}{2\rho^2} - \gamma. \tag{5}$$

The situation is slightly more complicated for p polarization, in which case α and γ can be numerically obtained as solutions of two algebraic equations. Originally reported in [10] and reduced to an equivalent but more appealing notation in [22], these equations are:

$$2\sqrt{2}\,t^2\sqrt{\alpha + \gamma} = \rho(1 + t^2)(t^2 + \gamma) - \sqrt{\rho^2(1 + t^2)^2(t^2 + \gamma)^2 - 4t^2(1 + \gamma)(t^4 + \gamma)}, \tag{6}$$

$$(1 + t^2)(1 + \rho)(t^2 + \gamma)\sqrt{\alpha + \gamma} = \sqrt{2}t^2\gamma \times (1 - 2\alpha + \gamma^2)\left[t^2(\gamma - 2\alpha) - \gamma^2 + t^4(t^2 + \gamma)\right]^2 \times$$
$$\left[t^6\left(2\alpha\gamma(2\gamma - 1) + \gamma^2(2\gamma^2 + 9\gamma + 5) - 4\alpha^2\right) + t^4\gamma\left(6\alpha\gamma + \gamma^2(5\gamma + 3) - 12\alpha^2\right) + \right.$$
$$\left. t^2\gamma^3(5\gamma - 8\alpha) + t^{10}\left(2\alpha + 2\gamma^2 + \gamma\right) + t^8\gamma(6\alpha + \gamma(4\gamma + 5)) - \gamma^5\right]^{-1}. \tag{7}$$

Equations (4) and (5) for s polarisation and Equations (6) and (7) for p polarisation enable the calculation of ϵ_r and ϵ_i (equivalently, n_r and n_i) at either polarisation state, from experimental input values (θ_c, R_c). This procedure is fully described in Ref. [10]. In what follows, we show how to eliminate reflectance R_c from the input, via its replacement by an additional critical angle θ_c', which may be accurately measured at an interface with a second prism.

3. Method's Description

Collecting two reflectance profiles by use of two different prisms introduces additional conditions to the problem. These conditions are already stated in Equation (1) ($n' = n\Lambda$ and $k' = k\Lambda$). By use of Equation (3), they can be written in the alternative form

$$F_1 = \frac{\alpha' + (t')^2}{1 + (t')^2} - \frac{\alpha + t^2}{1 + t^2} \cdot \Lambda^2 = 0, \tag{8}$$

$$F_2 = \frac{\sqrt{(\gamma')^2 - (\alpha')^2}}{1 + (t')^2} - \frac{\sqrt{\gamma^2 - \alpha^2}}{1 + t^2} \cdot \Lambda^2 = 0. \tag{9}$$

Throughout, accent marks denote parameters that relate to the second prism.

Parameters α, α', γ and γ' in Equations (8) and (9) are essentially functions of ρ, ρ', t and t' (equivalently, θ_c, θ_c', R_c and R_c'). These functions are given explicitly by Equations (4) and (5) for s polarisation, or implicitly by Equations (6) and (7) for p polarisation. In that

sense, Equations (8) and (9) define a system of two equations on four independent variables. Two of them are the measured input quantities (θ_c, θ'). The other two are the unknowns to be determined (R_c, R'_c). Solving numerically this system is the method's first step. To that end, we performed extensive numerical studies using Wolfram Mathematica's noniterative global solver `NSolve`, to conclude that the *real* roots are always unique, at least within the physically meaningful range $0 < R_c, R'_c < 1$.

Then, in the method's second step, the directly measured θ_c along with the numerically retrieved R_c enable the calculation of the complex optical constants via Equation (3). Exactly the same result is obtained by use of θ'_c and R'_c, instead.

Figure 2a depicts graphically the method's operating principle. Therein, the iso-θ_c curve is plotted in the (n, k) plane, representing the hypothetical measurement of a critical angle $\theta_c = 48.5°$ with the first prism; the critical angle measured with the second prism θ'_c (or equivalently, the angular shift Δ) varies in steps of $0.001°$, an amount that simulates the resolution of state-of-the-art rotary tables. Any given value of Δ defines a single point in the plot; its coordinates yield the sample's optical constants.
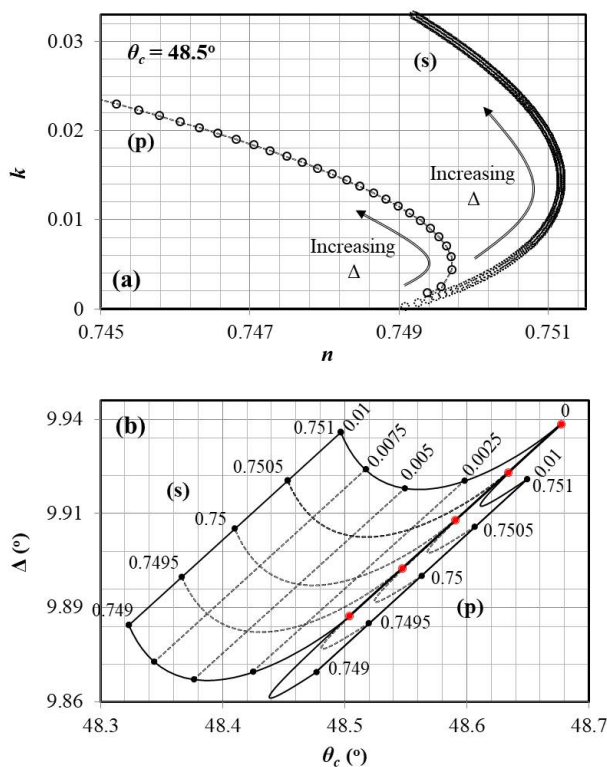
Figure 2. (**a**) Iso-θ_c curves in the (n, k) plane ($\theta_c = 48.5°$) arrows mark the direction of increasing Δ in steps of $0.001°$, starting from a base $\Delta = 9.882°$ ($9.845°$) for *s* (*p*) polarisation. (**b**) Iso-*n* and iso-*k* curves in the (θ_c, Δ) plane. Parameter *n* assumes constant values 0.749, 0.7495, 0.75, 0.7505 and 0.751 for both polarisations. Parameter *k* assumes constant values 0, 0.0025, 0.005, 0.0075 and 0.001 for *s* polarisation, as well as 0 and 0.01 for *p* polarisation. The common transparency line ($k = 0$) separates the *s* polarisation grid on the left, from the *p* polarisation grid on the right.

A complementary picture is drawn in Figure 2b, where families of iso-*n* and iso-*k* curves are plotted in the (θ_c, Δ) plane. Examining Figure 2 leads to several conclusions, the most important of which are the following. (1) For constant θ_c, k increases monotonically with increasing Δ; n does the same for low-k values, eventually reaching a characteristic turning point past which, n decreases with increasing Δ. (2) At the transparency limit ($k = 0$), curves for *s* and *p* polarisation converge into a single point (Figure 2a) or a single line (Figure 2b); there, the polarisation independent condition of total internal reflection holds true, that is $n = sin\theta_c$ and $n' = sin\theta'_c$. (3) The density of points in Figure 2a is lower

for *p* polarisation than it is for *s* polarisation. This observation is reflected in Figure 2b, where the grid pattern for *p* polarisation is more squeezed than it is for *s* polarisation. These facts are first indications that the method's sensitivity is generally higher with *s* polarised light, as we shall further discuss next.

4. Uncertainty Assessment

The distinctive advantage of the proposed method is that in its first step, reflectance R_c can be numerically computed from experimental input data (θ_c, θ_c') with higher accuracy than it can be directly measured. Uncertainty u_{R_c} in this computation can be expressed in terms of the input (P) and output (S) sensitivity matrices [31]

$$P = \begin{bmatrix} \dfrac{\partial F_1}{\partial \theta_c} & \dfrac{\partial F_1}{\partial \theta_c'} \\[2ex] \dfrac{\partial F_2}{\partial \theta_c} & \dfrac{\partial F_2}{\partial \theta_c'} \end{bmatrix}, \qquad S = \begin{bmatrix} \dfrac{\partial F_1}{\partial R_c} & \dfrac{\partial F_1}{\partial R_c'} \\[2ex] \dfrac{\partial F_2}{\partial R_c} & \dfrac{\partial F_2}{\partial R_c'} \end{bmatrix}, \tag{10}$$

where functions F_1 and F_2 are defined in Equations (8) and (9), respectively. The former definitions assume independence between the input variables θ_c and θ_c', which is reasonable, since these measurands are obtained via separate experimental runs. Then, it is

$$u_{R_c} = \sqrt{K_{11}^2 \cdot u_{\theta_c}^2 + K_{12}^2 \cdot u_{\theta_c'}^2} \tag{11}$$

where u_{θ_c}, $u_{\theta_c'}$ are the experimental uncertainties in the measurement of the respective critical angles, while K_{11}, K_{12} are the first row elements in the overall sensitivity matrix [31]

$$K = -S^{-1}P \tag{12}$$

Since the same experimental setup is to be used with both prisms, it is reasonable to assume that $u_{\theta_c'} \approx u_{\theta_c}$. We may thus define the normalised (with respect to u_{θ_c}) uncertainty

$$U_{R_c} = \frac{u_{R_c}}{u_{\theta_c}} = \sqrt{K_{11}^2 + K_{12}^2} \tag{13}$$

The preceding expressions can be used to evaluate under what circumstances errors in the numerical determination of R_c are (as we claim) smaller than corresponding errors in its direct measurement (the latter should be typically $> 1\%$). We shall skip this exercise to proceed right away with the investigation of a more interesting problem: the calculation of uncertainties in the determination of the complex optical constants from the directly measured θ_c and the indirectly retrieved R_c, during the method's second step. Based on standard error propagation rules and assuming zero covariance between θ_c and R_c, we may write for the relative uncertainties of n_r (or n) and n_i (or k)

$$\frac{u_{n_r}}{n_r} = \frac{u_n}{n} = \frac{1}{n} \cdot \sqrt{\left(\frac{\partial n}{\partial \theta_c} u_\theta \right)^2 + \left(\frac{\partial n}{\partial R_c} u_{R_c} \right)^2}, \tag{14a}$$

$$\frac{u_{n_i}}{n_i} = \frac{u_k}{k} = \frac{1}{k} \cdot \sqrt{\left(\frac{\partial k}{\partial \theta_c} u_\theta \right)^2 + \left(\frac{\partial k}{\partial R_c} u_{R_c} \right)^2}. \tag{14b}$$

It is now more convenient to define the normalised (with respect to u_{θ_c}) relative uncertainties of the real (U_{real}) and the imaginary (U_{im}) index which, by use of Equation (13), read:

$$U_{real} = \frac{u_{n_r}/n_r}{u_{\theta_c}} = \frac{1}{n} \cdot \sqrt{\left(\frac{\partial n}{\partial \theta_c} \right)^2 + \left(\frac{\partial n}{\partial R_c} \cdot U_{R_c} \right)^2}, \tag{15a}$$

$$U_{im} = \frac{u_{n_i}/n_i}{u_{\theta_c}} = \frac{1}{k} \cdot \sqrt{\left(\frac{\partial k}{\partial \theta_c}\right)^2 + \left(\frac{\partial k}{\partial R_c} \cdot U_{R_c}\right)^2}. \tag{15b}$$

For any given sample and prism pair, that is for fixed n, k and Λ, normalised relative uncertainties U_{real} and U_{im} can be calculated via Equation (15). Figure 3 depicts such calculations for indicative values $n = 0.75, \Lambda = 1.2$ and variable k. In agreement with the interpretation of Figure 2, we observe that the proposed method is generally more accurate for s, than it is for p polarisation. Another striking observation is that, within the k range we account for, the method's accuracy generally improves with increasing attenuation (that is, with increasing k). This seems to be a unique feature of our technique, since other approaches are typically expected to behave in the opposite way. Exceptionally, uncertainty U_{real} for p polarisation decreases with increasing k only up to a characteristic local minimum, thereafter increasing as attenuation grows. The local minimum may be interpreted as the equivalent of the turning point observed in Figure 2a. S polarisation exhibits the same behaviour at k values beyond the scale of the horizontal axis in Figure 3.
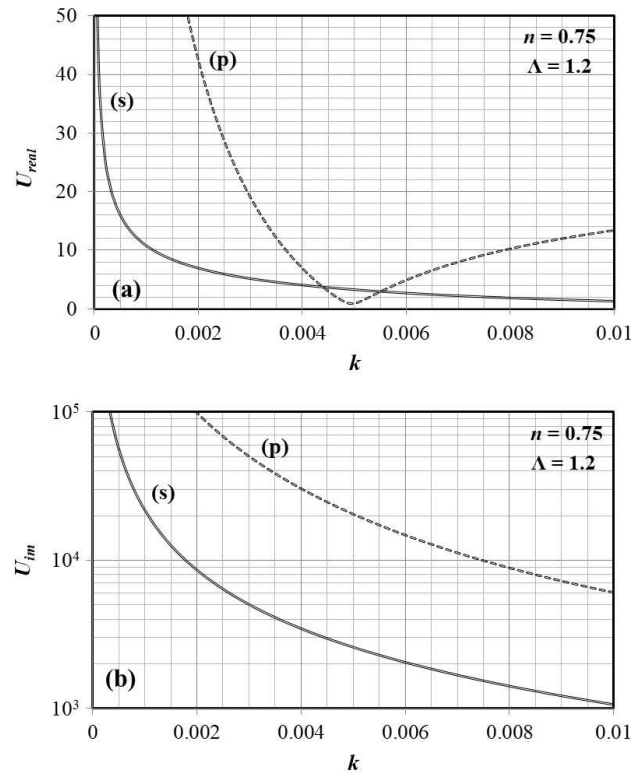
Figure 3. Normalized relative error U_{real} (**a**) and U_{im} (**b**) as a function of k, for both polarisation states. Throughout, we assume constant values for $n = 0.75$ and $\Lambda = 1.2$.

Modern refractometers equipped with high resolution rotary tables measure critical angles with an uncertainty u_{θ_c} between $0.001°$ and $0.005°$ (that is, between 20 µrad and 100 µrad). This uncertainty range is commonly assumed to be reasonable in the bibliography [22,32], suggesting that u_{θ_c} is primarily limited by the minimal incremental motion of the rotary table and remains practically insensitive to other factors, such as the divergence of the input laser beam or random noise (e.g., due to laser power fluctuations and the electronic detection system). It is also assumed that systematic errors in the measurement of critical angles, such as those resulting from the off-axis placement of the prism on the rotary table, have been properly removed (to that end, we remark that it is possible to calibrate the experimental setup with the use of a refractive index certified reference material).

Therefore, to estimate the magnitude of relative errors u_{n_r}/n_r and u_{n_i}/n_i we need to multiply U_{real} and U_{im} by a factor ranging from $2 \cdot 10^{-5}$ to 10^{-4}, respectively. As k approaches 0.01 for s polarisation (or the local minimum at $k \approx 0.005$ for p polarisation),

it is $U_{real} \approx 2$, indicating that u_{n_r}/n_r can be as low as $4 \cdot 10^{-5}$, or at least remain below $2 \cdot 10^{-4}$. Similarly, as k approaches 0.01, it is $U_{im} \approx 10^3$, suggesting that u_{n_i}/n_i should be in the range of 2% to 10% for s polarisation (increased five-fold for p polarisation).

Up to now, our assessment assumed fixed n and Λ. There exists some space for further error optimisation by proper choice of first and second prism, so as to tune n and Λ, respectively. In general, higher n and higher Λ values reduce the real and imaginary index error for s polarised light. For p polarisation, higher Λ values have the same effect; yet, a smaller n shifts the observed local minimum of the real index error to a lower k, an effect that might be desirable in several situations.

We shall not elaborate further on these dependencies, which however attest that the proposed method can determine the complex optical constants with relative uncertainties $u_{n_r}/n_r \sim 10^{-4}$ and $u_{n_i}/n_i \sim 10\%$, within a spectral range that extends from $k < 0.001$ to $k > 0.01$. These specifications compare well to standard refractometry with transparent samples (in terms of the real index), as well as ellipsometry (in terms of the imaginary index).

5. Limitations and Further Insights

The evident limitation in the practical use of our method relates to the confined attenuation span for which it remains highly accurate. However, even the narrow window, say, $0.001 < k < 0.01$, contains several material families of great scientific interest, ranging from food products and fuel oils to semiconductors, water and aqueous solutions (towards infrared wavelengths), as well as nearly the entirety of biological matter.

A second limitation that should be accounted for relates to the validity of Fresnel equations from which, the proposed mathematical framework originates. It is commonly accepted that, if light attenuation comes from absorption, Fresnel equations apply unconditionally. On the contrary, as is further elaborated in the bibliography [33,34], if light attenuation rises from scattering effects (that is, with inhomogeneus samples) Fresnel equations are valid only when the size of the scatterers remains small compared to the wavelength of light. Moreover, the applicability of the proposed method with inhomogeneous samples is further complicated by the fact that the same spot on the sample surface should be irradiated with both prisms.

A final aspect worth commenting on is the time duration of measurement; at first instance, one might assume that performing separate measurements on two different prisms may cause unwelcome delays. In reality, however, the proposed method spares the need for reflectance callibration, which is commonly required in prism coupling refractometry of attenuating media and involves a follow-up measurement at the prism–air interface. This simplification is due to the fact that critical angles θ_c and θ_c' can be determined by differentiating directly the uncalibrated reflectance profile, as is measured (in arbitrary units) by the photodiode.

6. Conclusions

This letter introduces two prism critical angle refractometry as a novel method for determining the complex optical constants of attenuating media, by means of a well-posed nonlinear equation system that can be solved numerically. The proposed method exhibits several appealing features, the most important of which are summarised below.

1. A pair of angles (θ_c, θ_c') is all that the method needs as input. To the benefit of precision, reflectance values are not required in the computational process.
2. The routine is general, since it applies with s and p polarised light, facilitating the characterisation of optically isotropic and anisotropic samples.
3. Uncertainty in the determination of the output quantities (n_r, n_i) decreases as attenuation grows from zero, which is ideally suited for analysing media that attenuate light as much as, for example, most forms of biological matter.

Uncertainty assessment indicated that the real (or the imaginary) index can be determined with a relative error $\sim 10^{-4}$ (or $\sim 10\%$), respectively. The method's specifications

meet the needs of several application in various fields, such as biomedical optics, analytical chemistry and quality control.

References

1. Bond, W.L. Measurement of the Refractive Indices of Several Crystals. *J. Appl. Phys.* **1965**, *36*, 1674–1677. [CrossRef]
2. Shukla, R.; Srivastava, A.; Srivastava, A.; Srivastava, M.; Dixit, S.; Misra, D. Design of an optoelectronic refractometer having an adjustable range of refractive index measurement. *Opt. Laser Technol.* **2008**, *40*, 692–696. [CrossRef]
3. Onodera, H.; Awai, I.; Ikenoue, J.I. Refractive-index measurement of bulk materials: Prism coupling method. *Appl. Opt.* **1983**, *22*, 1194. [CrossRef] [PubMed]
4. Russo, N.; Tonso, A.; Sicre, E. Liquid refractometry: An approach for a continuous measurement. *Opt. Laser Technol.* **1993**, *25*, 109–112. [CrossRef]
5. Sun, T.Q.; Ye, Q.; Wang, X.W.; Wang, J.; Deng, Z.C.; Mei, J.C.; Zhou, W.Y.; Zhang, C.P.; Tian, J.G. Scanning focused refractive-index microscopy. *Sci. Rep.* **2014**, *4*, 5647. [CrossRef] [PubMed]
6. Elshazly-Zaghloul, M.; Azzam, R.M.A. Brewster and pseudo-Brewster angles of uniaxial crystal surfaces and their use for determination of optical properties. *J. Opt. Soc. Am.* **1982**, *72*, 657. [CrossRef]
7. Luna-Moreno, D.; 1 De la Rosa-Cruz, E.; Cuevas, F.; Regalado, L.; Salas, P.; Rodríguez, R.; Castaño, V. Refractive index measurement of pure and Er^{3+}–doped ZrO_2–SiO_2 sol–gel film by using the Brewster angle technique. *Opt. Mater.* **2002**, *19*, 275–281. [CrossRef]
8. Pabitha, G.; Dhanasekaran, R. Investigation on the linear and nonlinear optical properties of a metal organic complex—Bis thiourea zinc acetate single crystal. *Opt. Laser Technol.* **2013**, *50*, 150–154. [CrossRef]
9. D'silva, E.; Podagatlapalli, G.K.; Rao, S.V.; Dharmaprakash, S. Structural, optical and electrical characteristics of a new NLO crystal. *Opt. Laser Technol.* **2012**, *44*, 1689–1697. [CrossRef]
10. Koutsoumpos, S.; Giannios, P.; Stavrakas, I.; Moutzouris, K. The derivative method of critical-angle refractometry for attenuating media. *J. Opt.* **2020**, *22*, 075601. [CrossRef]
11. Matiatou, M.; Giannios, P.; Koutsoumpos, S.; Toutouzas, K.G.; Zografos, G.C.; Moutzouris, K. Data on the refractive index of freshly-excised human tissues in the visible and near-infrared spectral range. *Results Phys.* **2021**, *22*, 103833. [CrossRef]
12. Humphreys-Owen, S.P.F. Comparison of Reflection Methods for Measuring Optical Constants without Polarimetric Analysis, and Proposal for New Methods based on the Brewster Angle. *Proc. Phys. Soc.* **1961**, *77*, 949–957. [CrossRef]
13. Azzam, R.M.A.; Ugbo, E.E. Contours of constant pseudo-Brewster angle in the complex e plane and an analytical method for the determination of optical constants. *Appl. Opt.* **1989**, *28*, 5222. [CrossRef] [PubMed]
14. Tioua, B.; Soltani, M.T.; Khechekhouche, A.; Wondraczek, L. Physical properties and luminescence of highly stable erbium-doped antimony glasses for NIR broadband amplification. *Opt. Laser Technol.* **2022**, *152*, 108152. [CrossRef]
15. Neethish, M.; Kumar, V.R.K.; Nalam, S.A.; Harsha, S.S.; Kiran, P.P. Effect of chirp on supercontinuum generation from Barium Zinc Borate glasses. *Opt. Laser Technol.* **2022**, *149*, 107890. [CrossRef]
16. Mahadevan, M.; Sankar, P.; Vinitha, G.; Arivanandhan, M.; Ramachandran, K.; Anandan, P. Non linear optical studies on semiorganic single crystal: L-arginine 4-nitrophenalate 4-nitrophenol dihydrate (LAPP). *Opt. Laser Technol.* **2017**, *92*, 168–172. [CrossRef]
17. Zheng, J.; Jiang, J.; Chen, H.; Zheng, R.; Shen, X.; Yu, K.; Wei, W. Optical nonlinearity and supercontinuum generation of tellurite glass at 1.064 μm. *Opt. Laser Technol.* **2021**, *138*, 106832. [CrossRef]
18. Koutsoumpos, S.; Giannios, P.; Moutzouris, K. Extended derivative method of critical-angle refractometry for attenuating media: Error analysis. *Meas. Sci. Technol.* **2021**, *32*, 105007. [CrossRef]
19. Koutsoumpos, S.; Giannios, P.; Moutzouris, K. Critical Angle Refractometry for Lossy Media with a Priori Known Extinction Coefficient. *Physics* **2021**, *3*, 569–578. [CrossRef]
20. Azzam, R.M.A. Analytical determination of the complex dielectric function of an absorbing medium from two angles of incidence of minimum parallel reflectance. *J. Opt. Soc. Am. A* **1989**, *6*, 1213. [CrossRef]
21. Hirschfeld, T. Accuracy and Optimization of the Two Prism Technique for Calculating the Optical Constants from ATR Data. *Appl. Spectrosc.* **1970**, *24*, 277–282. [CrossRef]

22. Koutsoumpos, S.; Giannios, P.; Moutzouris, K. Critical angle refractometry with optically isotropic attenuating media. *Appl. Phys. B* **2022**, *128*, 91. [CrossRef]

23. Giannios, P.; Toutouzas, K.G.; Matiatou, M.; Stasinos, K.; Konstadoulakis, M.M.; Zografos, G.C.; Moutzouris, K. Visible to near-infrared refractive properties of freshly-excised human-liver tissues: Marking hepatic malignancies. *Sci. Rep.* **2016**, *6*, 27910. [CrossRef] [PubMed]

24. Giannios, P.; Koutsoumpos, S.; Toutouzas, K.G.; Matiatou, M.; Zografos, G.C.; Moutzouris, K. Complex refractive index of normal and malignant human colorectal tissue in the visible and near-infrared. *J. Biophotonics* **2016**, *10*, 303–310. [CrossRef]

25. Niskanen, I.; Räty, J.; Peiponen, K.E. Complex refractive index of turbid liquids. *Opt. Lett.* **2007**, *32*, 862. [CrossRef] [PubMed]

26. Sun, J.; Wang, J.; Liu, Y.; Ye, Q.; Zeng, H.; Zhou, W.; Mei, J.; Zhang, C.; Tian, J. Effect of the gradient of complex refractive index at boundary of turbid media on total internal reflection. *Opt. Express* **2015**, *23*, 7320. [CrossRef] [PubMed]

27. Räty, J.; Pääkkönen, P.; Peiponen, K.E. Assessment of wavelength dependent complex refractive index of strongly light absorbing liquids. *Opt. Express* **2012**, *20*, 2835. [CrossRef]

28. Calhoun, W.R.; Maeta, H.; Combs, A.; Bali, L.M.; Bali, S. Measurement of the refractive index of highly turbid media. *Opt. Lett.* **2010**, *35*, 1224. [CrossRef]

29. Goyal, K.G.; Dong, M.L.; Nguemaha, V.M.; Worth, B.W.; Judge, P.T.; Calhoun, W.R.; Bali, L.M.; Bali, S. Empirical model of total internal reflection from highly turbid media. *Opt. Lett.* **2013**, *38*, 4888. [CrossRef]

30. Guo, W.; Xia, M.; Li, W.; Dai, J.; Zhang, X.; Yang, K. A local curve-fitting method for the complex refractive index measurement of turbid media. *Meas. Sci. Technol.* **2012**, *23*, 047001. [CrossRef]

31. Beck, B.T.; Peterman, R.J.; Wu, C.H.J. The Uncertainty in Solutions to Implicit Equation Systems. *J. Fluids Eng.* **2019**, *142*, 014502. [CrossRef]

32. Garcia-Valenzuela, A.; Pena-Gomar, M.; Fajardo-Lira, C. Measuring and sensing a complex refractive index by laser reflection near the critical angle. *Opt. Eng.* **2002**, *41*, 1704–1716. [CrossRef]

33. García-Valenzuela, A.; Barrera, R.G.; Sánchez-Pérez, C.; Reyes-Coronado, A.; Méndez, E.R. Coherent reflection of light from a turbid suspension of particles in an internal-reflection configuration: Theory versus experiment. *Opt. Express* **2005**, *13*, 6723. [CrossRef] [PubMed]

34. Morales-Luna, G.; Contreras-Tello, H.; García-Valenzuela, A.; Barrera, R.G. Experimental Test of Reflectivity Formulas for Turbid Colloids: Beyond the Fresnel Reflection Amplitudes. *J. Phys. Chem. B* **2016**, *120*, 583–595. [CrossRef]